Monthly-Scale Extended Predictions Using the Atmospheric Model Coupled with a Slab-Ocean

Zhenming Wang[1,2], Shaoqing Zhang[*1,2,3], Yishuai Jin[1,2], Yinglai Jia[1], Yangyang Yu[1,2], Yang Gao[3,4], Xiaolin Yu[1,2,3], Mingkui Li[1,2,3], Xiaopei Lin[1,2,3], Lixin Wu[1,2,3],

[1] Key Laboratory of Physical Oceanography, Ministry of Education, Institute for Advanced Ocean Study, Frontiers Science Center for Deep Ocean Multispheres and Earth System (DOMES), Ocean University of China, Qingdao, 266100, China
[2] College of Oceanic and Atmospheric Sciences, Ocean University of China, Qingdao, 266100, China
[3] Pilot National Laboratory for Marine Science and Technology, Qingdao, 266100, China
[4] Key Laboratory of Marine Environment and Ecology, and Frontiers Science Center for Deep Ocean Multispheres and Earth System (FDOMES), Ministry of Education, Ocean University of China, Qingdao 266100, China

Correspondence to: Shaoqing Zhang (szhang@ouc.edu.cn)

Abstract. Given the good persistence of sea surface temperature (SST) due to the slow-varying nature of the ocean, an atmospheric model coupled with a Slab Ocean Model (SOM) instead of a 3-D dynamical ocean model is designed as an efficient approach for extended-range predictions. The prediction experiments from July to December 2020 are performed based on the Weather Research and Forecasting (WRF) model coupled to the SOM (WRF-SOM) with the initial and boundary conditions same as the WRF coupled to the Regional Ocean Model System (WRF-ROMS). The WRF-SOM is verified to have better performance of SSTs in the extended-range predictions than WRF-ROMS since it avoids the complicated model biases from the ocean dynamics and seabed topography when extended-range predictions are made using a 3-D dynamical ocean model. The improvement of SSTs can lead to the remarkable impact on the response of the atmosphere from the surface to the upper layer. Taking typhoon as an example of extreme events, the WRF-SOM can obtain comparable intensity predictions and slightly improved track predictions due to the improved SSTs in the initialized WRF-SOM system. Overall, the WRF-SOM can ensure the stability of extended-range prediction and reduce the demand for computing resources by roughly 50%.

1 Introduction

Extended-range predictions fill the gap between weather and climate predictions. Recent research has demonstrated kinds of sources of predictability for the extended period such as the Madden-Julian Oscillation (MJO), the evolution of El Niño-Southern Oscillation, soil moisture, snow cover, sea ice, stratosphere-troposphere interactions, ocean conditions, and tropical-extratropical teleconnections (Wheeler and Hendon, 2004; Vitart and Robertson, 2018). As a growing demand from the applications community and progress in identifying and simulating key sources of extended period (Vitart, 2014; White et al., 2017), it is worthwhile improving forecast skills for monthly-scale extended period predictions to realize the social security, disaster early warning, agricultural management, and water resource management (David, 2010).

In the extended period prediction, sea surface temperature (SST) is one of the most important information provided by the oceanic model to the atmospheric model in the air-sea interaction. For instance, tropical SST plays an important role in controlling the weather/climate worldwide by various teleconnection effects (David, 2010). Dian et al. (2013) demonstrated the importance of air-sea interaction to the atmospheric mesoscale processes by comparing the response of the precipitation to the SST between the coupled and uncoupled models. Furthermore, Stan (2018) emphasized that the SST anomaly can directly lead to the change in the convection intensity.

The ocean-atmosphere coupling has an important impact on the extended-range prediction skills (Vitart and Molteni, 2010). Rashid et al. (2019) adopted the Bureau of Meteorology unified atmospheric model (BAM) coupled with the Australia Community Ocean Model (ACOM) to predict the MJO and proposed that actual MJO prediction skills may be further improved through continued development of the dynamical prediction system. The coupled ocean-atmosphere models are mainly used for numerical simulation and prediction in the extended period (Saravanan and Chang, 2019).

However, there are some inherent defects for the specific problems in extended-range prediction using atmosphere-ocean coupled models. For instance, the 3-D dynamical ocean model inevitably introduces unnecessary biases from the seabed topography, which can transport from bottom to surface during prediction (Wu et al., 1997). Due to the existence of seabed topography with finite amplitude, the wave models in a linear system are no longer independent of each other, resulting in coupling between models. This coupling effect between models acts on the circulation field in different ways, making the simple linear superposition of models no longer truly reflect the oceanic circulation field structure. The effects of seabed topography on the baroclinic model should be stronger. Therefore, the seabed topography can indirectly affect the SST through the circulation field. The 3-D dynamical ocean model coupled to the atmospheric model can have cold drift during the extended-range prediction period due to the overestimation of latent heat in the coupled model (Ren and Qian, 2010). In addition, the sensitivity of ocean thermodynamics to the ocean dynamics leads to the enhancement of mixing in the upper ocean and indirectly reduces SST (Hu et al., 2017). In general, the errors of 3-D dynamical ocean models can be specific to different system configurations. The model resolution is another way affecting the SST prediction, which is verified that the biases can be slightly eliminated in the Kuroshio extension area with the increase in model resolution (Li et al., 2020). Therefore, European Centre for Medium-Range Weather Forecasts (ECMWF) summarized and evaluated the results during

the extended period prediction, and proposed that the improvement of extended-range prediction should be accompanied by the significant reduction of SST biases in a coupled model (Palmer et al., 1990). In total,based on the good persistence of SST, we can simplify the SST evolution process to avoid biases from the ocean dynamics and seabed topography (Zuidema et al., 2016).

70 Considering that SST is an important variable affecting air-sea interactions and 3-D dynamical ocean models have a deficiency in the SST prediction during the extended period, one possible way to improve this period prediction is that, we only focus on the SST as the bottom boundary of atmospheric model for the extended-range prediction research. The SST has good persistence in the extended period and only the thermal effect needs to be considered (the time scale of ocean circulation is relatively long). According to that, the Slab Ocean Model (SOM) can be utilized as the ocean model for

75 extended-range prediction such that biases of SST are easier to manage (Zuidema, 2016). More importantly, the SOM can greatly reduce the computing expense and obtain the forecast results more quickly, which can provide a more economical and efficient method for further study.

In this paper, we develop a new approach using atmospheric model coupled with a Slab Ocean Model (WRF-SOM) to do monthly-scale extended-range predictions. For comparison of the prediction results of WRF-SOM, we also carry out the

80 forecast experiments using WRF coupled to the Regional Ocean Model System (ROMS) based on the regional coupled prediction system for the Asia-Pacific (AP-RCP) developed by Li et al. (2020). Firstly, by comparing the performances of SST predictions in the WRF-SOM and WRF-ROMS, we show the rationality of WRF-SOM in the extended-range predictions. WRF-SOM can avoid the influence of cold deviation at the subsurface in WRF-ROMS on SST in extended period. Secondly, we discuss the response of atmosphere (e.g., the air temperature, and geopotential height) on SSTs to

85 identify the improvement of WRF-SOM compared with WRF-ROMS in the cold deviation area. Finally, taking typhoons as the representation of the extreme weather events, we track the differences of typhoon paths and maximum wind speed (MWS) between WRF-ROMS and WRF-SOM and suggest that the performances of typhoon predictions are basically consistent in the two models during the extended period.

The rest of the paper is organized as follows. Section 2 details the source of SST biases, the brief introduction of WRF-SOM

90 and WRF-ROMS, the experiment implementation, and the data sources. Section 3 evaluates the feasibility of SST predictions in WRF-SOM, compares the response of the atmosphere to SSTs in WRF-SOM and WRF-ROMS, and verifies the rationality of WRF-SOM in typhoon predictions. Finally, the summary and discussion are given in Section 4.

2 Methodology

2.1 Brief introduction of WRF-ROMS coupled model

95 In this study, we use the high-resolution WRF-ROMS coupled system for comparison (Li et al., 2020). The system covers the area of the Asia-Pacific, which consists of 27 km WRF, 9 km ROMS, and observational information through dynamically downscaling coupled assimilation. The vertical layers of WRF and ROMS are 28 and 33 respectively. The time

step for both WRF and ROMS is 60 s, the coupled interval time between ocean and atmosphere is 600 s, and the forecast lead time is 34 days for each case. The system is initialized from the Climate Forecast System Version2 reanalysis (CFSv2) (Saha et al., 2014), on January first, 2016, and spun up for two years. For the ocean component, in model-based analysis products, the prediction system has similar quality with CFSv2 and HYCOM in temperature and salinity characteristics, and has been verified by Argo observation. For the atmosphere component, the forecast system also has the similar forecast skills as CFSv2, National Centers for Environmental Prediction-Global Ensemble Forecast system (NCEP-GEFS) and European Centre for Medium-Range Weather Forecasts-Ensemble Prediction System (ECMWF-EPS), especially in precipitation forecasting. The operational system has realized the extended-range prediction of atmospheric and oceanic environments and serves as an effective research platform to study the influence of model resolution on typical mesoscale atmospheric and oceanic phenomena in the Asia-Pacific area. The high-resolution prediction system enhances the capability of atmosphere-ocean coupled models to describe many local details, which is a necessary step to discuss the predictability in the extended period.

2.2 Slab-Ocean scheme in a coupled model

In order to describe the response of the upper ocean to the surface wind, a simple model—SOM is given (Raymond et al., 1973). Compared with the 3-D dynamical ocean model, the ocean mixed layer temperature is the only prognostic state variable for the SOM to represent the SST. Jia et al. (2019) adopted the SOM to study the ocean mesoscale variability. The related prognostic equation is the first law of thermodynamics for the ocean mixed layer given by Eq.(1):

$$\rho C_p h_{mix} \frac{\partial T_{mix}}{\partial t} = Q_{atm} - Q_{ocn} , \qquad (1)$$

where ρ is the ocean water density, C_p is the specific heat capacity of the ocean water, h_{mix} is the depth of the mixed layer, T_{mix} is the mixed layer temperature, Q_{atm} is the net surface heat flux from the atmosphere to the mixed layer, and Q_{ocn} is the net heat transfer from mixed-layer column to the subsurface, which is calculated by mixed layer depth and temperature lapse rate. Eq.(2) shows the heat budget of the sea surface from the atmosphere:

$$Q_{atm} = Q_{sol} - Q_l - Q_{sen} - Q_{latent} , \qquad (2)$$

where Q_{sol} is the net radiative heating of the ocean mixed layer by solar radiation, Q_l is the net longwave radiative cooling of the ocean mixed layer, Q_{sen} is the net sensible heat flux from the ocean to the atmosphere, Q_{latent} is the net latent heat flux from the ocean to the atmosphere. Q_{atm} and Q_{ocn} are calculated synchronously with the prediction time in the model. Eq.(3) shows the effect of Coriolis force and wind stress in the mixed layer:

$$\begin{aligned} \frac{\partial h_u}{\partial t} &= f \times h_v + \tau_x \\ \frac{\partial h_v}{\partial t} &= -f \times h_u + \tau_y \end{aligned} , \qquad (3)$$

where h_u (h_v) is the τ_x-driven (τ_y-driven) momentum in the ocean mixed layer, f is Coriolis force, and τ_x and τ_y are respectively the zonal and meridional components of wind stress at the surface. Eq.(3) is calculated by time-centering difference and Eq.(4) shows the variations of ocean mixed layer depth, which is affected by the wind stress and heat flux:

$$h_{mix} = \frac{Q_{atm} - Q_{ocn}}{\Gamma} + \sqrt{\frac{(Q_{atm} - Q_{ocn})^2}{\Gamma^2} + \frac{2 \times (h_{u2}^2 + h_{v2}^2)}{\Gamma g \alpha}}, \tag{4}$$

where h_{mix} is the mixed layer depth, g is the gravitational acceleration, Γ is the lapse rate of the water temperature, and α is the thermal expansion coefficients.

Such basic driving processes of WRF-SOM and the relationship between the variables can be illustrated in **Fig. 1**. The SOM is driven by the surface wind, sea surface heat flux, and heat conduction between the mixed layer and subsurface. The mixed layer depth is determined by the surface wind stress (τ_x and τ_y) and the heat budget (Q_{atm} and Q_{ocn}) in the mixed layer. Both the enhancement of surface wind stress and heat flux to the mixed layer will lead to the deepening of the mixed layer depth. When the ocean surface is heated, there will be a temperature gradient from sea surface to the areas beneath it. With the wind stirring the upper layer, an almost uniform layer is formed, and there is a density gradient below the mixed layer. In the upper mixed layer, the temperature is independent of depth. We assume that once the initial delamination is destroyed in this layer, it will mix to a completely uniform state. It means that the ocean temperature is well-mixed and the SST is considered the same as T_{mix}.

Although the SOM has the advantages of computational stability, easy control of error sources and low computational consumption, it is worth to mention that the SOM is driven only by surface wind and does not include the simulation of 3-D ocean dynamical processes.

2.3 Implementation, data source (including model setting and initial condition sources), and data processing method

In this study, the WRF version WRF3.7.1 and the ROMS version ROMS3.8 is applied (Skamarock et al., 2008; Shchepetkin and Mcwilliams, 2005). The boundary condition of the forecast is interpolated from the CFSv2 forecast data set. The WRF-ROMS is initialized from the CFSv2 reanalysis at 00 UTC on 1st January 2016, spun up for two years with the CFSv2 background boundary conditions, and applies the weakly coupled data assimilation approach (WCDA). The atmospheric and oceanic components conduct their own data assimilation procedure within the coupled model framework. The WCDA begins on 00 UTC 1 January 2018 after the 2-year spin up. The atmospheric model uses standard 3-dimensional variational data assimilation (3D-Var) to further combine atmospheric observations and the oceanic model adopts multi-scale 3D-Var to assimilate the profiles of temperature and salinity. Then, the states are constrained by cycling through the real-time operational data assimilation processes with updated observations every 6 hours for the atmosphere and 24 hours for the

ocean, providing initial conditions for the routine forecasts. The simulation region covers the Asia-northwest Pacific and North Indian Ocean (74° E-180° E, 18° S-60° N). The forecasts are made every day from July 19th to December 31st 2020. Each case generates a 34-day forecast for the atmosphere and ocean environment.

The WRF-SOM is completely consistent with WRF-ROMS in atmospheric model settings and the grid of SOM is consistent with the atmospheric model. The forecast cases made by WRF-SOM are same to the WRF-ROMS expect for roughly 20 cases/days are missed, which is caused by hardware damage and untimely release of boundary information. Li and Ding (2011) proposed that the linear relationship between the predictability limit and the logarithm of initial error holds only in the case of relatively small initial errors. If the initial errors are large, the growth of mean error would directly enter into the nonlinear phase. Therefore, for each experiment, we keep the initial and boundary conditions of the WRF-SOM in the atmosphere and ocean the same as those in the WRF-ROMS and assure that the forecast lead time of each experiment is over one month.

The Hybrid Coordinate Oceanic Circulation Model (HYCOM) reanalysis (https://www.hycom.org) used in this study is provided by Naval Research Laboratory (Cummings and Smedstad, 2013). The horizontal resolution of HYCOM reanalysis reaches 0.08° and the time interval is 6 hours, which is relatively stable and highly matched with our forecast system. In addition, considering the HYCOM reanalysis being a mature and widely recognized analysis system, the global reanalysis can be a good choice to verify the model prediction performances (Srinivasan et al., 2011; Chassignet et al., 2003). The typhoon observations are from the National Meteorological Center (NMC) of China (http://typhoon.nmc.cn/web.html). The validation data of the atmospheric component is from CFSv2 (https://rda.ucar.edu/datasets/ds094.1/). All the simulation experiments use the computing nodes configured with 24 central processing unit (CPU) cores, 2.6 GHz dominant frequency, and 256 GB of global DDR4 memory.

The predictability of SST in WRF-ROMS and WRF-SOM is evaluated by the root mean square error (RMSE) and the anomaly correlation coefficient (ACC), which is written as follows:

$$RMSE_j = \sqrt{\frac{1}{M}\sum_{i=1}^{M}(x_{i,j} - f_{i,j})}\ , \tag{5}$$

$$ACC_j = \frac{\sum_{i=1}^{M}(x_{i,j} - \overline{x_j})\times(f_{i,j} - \overline{f_j})}{\sqrt{\sum_{i=1}^{M}(x_{i,j} - \overline{x_j})^2 \times \sum_{i=1}^{M}(f_{i,j} - \overline{f_j})^2}}\ , \tag{6}$$

where $x_{i,j}$ is the forecast value, $f_{i,j}$ is the reanalysis data, $\overline{x_j}$ is the spatial average of the forecast value, $\overline{f_j}$ is the spatial average of the truth value, and $i = 1,2,3...M$ and $j = 1,2,3....N$ represent grid points and time series respectively.

3 Comparing the forecast results of WRF-SOM with WRF-ROMS

3.1 Predictability of sea surface temperature and bias

The prediction skills of SST in the WRF-SOM and WRF-ROMS have been assessed by calculating the RMSE averaged of 142 forecast cases from July to December. **Figure 2a** shows the RMSE of SSTs in the WRF-SOM is generally lower than that in the WRF-ROMS and both forecast errors increase with the lead time. The maximum different value of the RMSEs variation between the WRF-SOM and WRF-ROMS occurs in 20-25 days. The averaged values of the SST errors in both models are within 1.4°C during the forecast period and the RMSEs of 75% forecast cases in WRF-SOM are better than those in WRF-ROMS, as shown in **Fig. 2b**. Moreover, the bias in the WRF-SOM grows more slowly than that in the WRF-ROMS. Only at the start of the forecasts, the errors of SST in WRF-ROMS are lower than that in WRF-SOM. It is because the errors in the 3-D dynamical ocean model have not spread from subsurface to the surface and initial condition still plays a major role (Lekshmi et al., 2022). Except for July and August, the SST error growth rate is faster in WRF-SOM over different months in the second half of the year. From September to December, the prediction of SST in WRF-ROMs after 30 days begins to take advantage, which may be caused by the dynamic processes such as ocean circulation beginning to dominate the factors of SST prediction as the time scale becomes larger, as shown in Fig. 2e. We also notice that the WRF-SOM simulated SST has larger errors than the WRF-ROMS' in July. Further analyses show that this large errors are associated with the nature that the SOM lacks ocean 3-D dynamical and thermodynamical processes. For example, the major SST errors distribute over the Large Meander of Kuroshio (Yang et al., 2012) and the lack of ocean dynamics could reduce the horizontal energy transport to a certain extent (Shell, 2013). The biggest difference of SST RMSEs in WRF-ROMS and WRF-SOM occurs in September, October and November, which also shows that sea ice is not the main reason for the large cold deviation in WRF-ROMS. In order to match the configuration in the ROMS without sea-ice component currently, in this study we did not include sea-ice, although the sea-ice parameterization in the SOM is available. In the future study, it may be necessary to include sea-ice in SOM, which may have influences on middle and high latitudes.

To explore the spatial distribution of skills with different forecast periods in WRF-SOM, we use the ACC of SST anomaly to characterize the temporal and spatial predictability of SST in the WRF-SOM and WRF-ROMS (Wu et al., 2016). **Figure 2c** shows that their overall ACC can reach more than 0.75 during the 34-day forecasts and the performance of the WRF-SOM in the whole domain is higher than that of WRF-ROMS. Meanwhile, the ACC in 74% forecast cases in WRF-SOM is better than those in WRF-ROMS, as shown in **Fig. 2b**. Finally, **Figure 3a** and **3b** show the forecast SSTs in WRF-ROMS have an obvious cold deviation in the area around the Kuril Islands and the Sea of Okhotsk (35° N-58° N, 140° E-160° E). Although the cold deviation in WRF-ROMS exists every month in the second half of the year in this region, lack of sea-ice model and inappropriate boundary conditions may aggravate the cold deviation in this area, which needs more experiments to validate.

In order to explore the spatial distribution of SST prediction skills in the two models, especially in the cold deviation area, we calculate ACC of SSTs at each grid point. Through the spatial distribution of ACC displayed in **Fig. 4** in different forecast periods, it is found that the mean biases of WRF-SOM and WRF-ROMS decreases with time in the whole area.

Since the initial state of the ocean can be maintained for a period of time in the simulation, the main patterns of the ACC are consistent in the two models, and the value increases with the latitude significantly. The higher skills of WRF-SOM are mainly concentrated in the area north of 15°N compared with WRF-ROMS. Over 60% grid points in the simulation area have higher ACC values of SST in WRF-SOM, and the proportion rises slightly with the prediction time (green dots in the right column of **Fig. 4**). Focused on the cold deviation area in the green rectangle, the proportion reaches more than 80% (red dots in the right column of **Fig. 4**). In summary, the performance of SSTs in the WRF-SOM is more reasonable than the WRF-ROMS in terms of temporal variation and spatial distribution of predictability.

In order to explore the causes of cold deviation area in WRF-ROMS, the variations of averaged error of SST and the water temperature at the subsurface are shown. **Figure 5a-5c** identifies the comparison of averaged mixed layer depth during the prediction period. The mixed layer depth in WRF-ROMS and HYCOM are both calculated by the depth at which the difference from SST is 0.2 ℃. The mixed layer depth in WRF-ROMS is significantly greater than that in WRF-SOM and the reanalysis data from HYCOM. Moreover, the cold deviation of WRF-ROMS at the subsurface continues to conduct upward with the forecast time, and finally the predicted value of SST is low in this area as shown in **Fig. 5d** and **5e**. Lack of vertical convection and Ekman pumping effect in the SOM can enhance this surface heat residence effect even more in WRF-SOM forecasts. The abnormal cold deviation at the subsurface may be caused by the imperfect data assimilation scheme, imprecise ocean processes, and insufficient resolution of the coupled model (Benjamin and Daniel, 1993; Chen et al., 2013; Xu et al., 2022). These issues require more research work to further clarify in the follow-up studies.

3.2 Impact on Extended-range Predictions

The SST differences between WRF-ROMS and WRF-SOM spread rapidly in all prediction cases and have obvious thermodynamic feedback to the atmosphere. For instance, the region with a large deviation of SST is expected to have a great impact on the atmospheric process (Hao et al., 2016). The first mode of SST and air temperature at 850 hPa is verified to be positively correlated in most of the East China Sea (Zeng et al., 2010). As shown in **Fig. 6**, the air temperature at the surface is directly affected by the SSTs and there is a strong cold deviation of more than 5 ℃ in the WRF-ROMS in the Sea of Okhotsk and Kuril Islands during the extended period. The errors of air temperature at the surface in the Sea of Okhotsk and Kuril Islands of WRF-SOM are within 3 ℃ in the extended period, which is much closer to the CFSv2 reanalysis compared with WRF-ROMS.

Since the main deviation between WRF-ROMS and WRF-SOM mainly comes from the sea surface, in order to explore the influence of SST on the whole atmosphere, we study the variation of RMSEs of air temperature and geopotential height (GPH) with different heights to characterize the stability of the subtropical high and the upper atmosphere (Lu and Lin, 2009; Zhou and Yu, 2009). The RMSEs of air temperature increase with height, and the differences between the two models are the biggest at the surface (**Fig. 7a**). The deviation of air temperature gradually disappears when reaching the height of 300 hPa (**Fig. 6b**). The RMSEs of the GPH also increase with the height (**Fig. 8a**). However, the differences between the two models are opposite to the temperature and increases with the height (**Fig. 8b**). Compared with the WRF-ROMS, the WRF-

SOM performs better in the forecast of the GPH field in the high, middle, and low atmosphere, as shown in **Fig. 8**. The difference between the RMSEs of GPH in the two models are increasing from the lower level to the upper level, which means that the deviation between the WRF-SOM and the WRF-ROMS is generated from the surface and propagates to the upper layer. Therefore, combined with the results of air temperature and GPH, the response of variables with different physical properties to SST will also appear in different states. In terms of the extended-range prediction, WRF-SOM has obvious advantages in the areas around the Kuril Islands and the Sea of Okhotsk, where WRF-ROMS has large deviation in SSTs.

3.3 The prediction of tropical cyclones in extended-range scales

Typhoon is an important extreme weather phenomenon in the extended-range forecast, and the typhoon in the Western Pacific has a profound impact on coastal countries (Webster et al., 2014). The typhoon processes are deeply affected by the air-sea interaction, which can cover timescales from days to weeks. Therefore, typhoons are selected as an example of the extreme weather to discuss the atmospheric predictability in the extended period. Following previous studies (Webster et al., 2014), we use track and intensity as the key prediction parameters. As the typhoon simulation from August to October 2020 (**Fig. 9a-9j**), the WRF-SOM can also obtain slightly better prediction paths than the WRF-ROMS after abandoning the ocean dynamics framework during the typhoon season. The results of typhoon tracking in the WRF-SOM are better than those in the WRF-ROMS within 72 hours during the processes of typhoons, as shown in **Table 1**. The simulation of typhoon tracks is mainly dominated by steering flow in the atmosphere model, and the improvement of SST can only slightly optimize the path (Anthes, 1982; Hollland, 1983) such that the forecast results are similar in WRF-SOM and WRF-ROMS. **Figure 10a-10j** show the performances of MWS of 11 typhoons from August to October in 2020, both in WRF-SOM and WRF-ROMS. Both systems are unable to achieve accurate simulation for super typhoons exceeding 40 m/s. However, BAVI has better MWS performances in WRF-SOM than in WRF-ROMS, as shown in **Fig. 10e**. We find that in the process of model simulation, the typhoon MWS is positively correlated with the SST, which can be caused by the surface heat flux and the surface water vapor. Among the eleven typhoons including three super ones, there is little difference in typhoon MWS between the WRF-SOM and the WRF-ROMS, which means that both the 3-D dynamical ocean model and the SOM have defects on the simulation of high-intensity typhoons. As for typhoon simulation, WRF-SOM can obtain comparable prediction results with WRF-ROMS. The analyses in section 3.1 show that the SST in SOM has large errors in July. It could cause the corresponding deviation in the air-sea interaction, and may have influence on typhoon activities (Potter et al., 2017). Since no typhoon is found in the examined July, adverse impacts of such SST errors on typhoons need to be paid particular attention.

4 Summary and discussion

In this study, to improve the numerical model predictability of monthly extended-range scales, we use the simplified SOM to

restrict the SST bias. It is because the 3-D dynamical ocean model inevitably introduces complex biases from the dynamics and seabed topography. Therefore, the experiments are implemented with the WRF-ROMS and WRF-SOM to investigate the SST deviation in the extended-range period and the associated atmosphere responses. We systematically evaluate the SST prediction effect of the WRF-SOM and the WRF-ROMS against the HYCOM reanalysis. As for SST prediction, WRF-

290 SOM can manage with the more specific errors than 3-D dynamical ocean models in some regions with complex and diverse heat budget, because it can effectively avoid the deviation from deep layers in 3-D dynamical ocean models. Furthermore, the reduction of SST biases in the WRF-SOM has a significant impact on the atmosphere at the surface, which not only affects the air temperature but also indirectly changes the GPH field in the middle and upper layer of the atmosphere. The WRF-SOM can obtain the compatible typhoon path and maximum wind speed predictions with WRF-ROMS and reduce the

295 consumption of computing resources by roughly 50%.

It is shown by our experiments that the subsurface modeling errors in the 3-D dynamical ocean model could propagate to the surface with the forecast lead time and make a large deviation in SST. To improve the predictability in the extended period, it is of vital importance to constrain the deviation of SST. Based on the good persistence of SST, it is verified that using the SOM instead of the 3-D dynamical ocean model can relieve the problem of rapid error growth in the prediction of SST in

300 some regions, and save a lot of computing resources. For the extreme weather event such as typhoons, the predictions of WRF-SOM are in good agreement with WRF-ROMS. However, the WRF-SOM also has its own limitations. The overall simulation of SST in WRF-SOM is relatively stable. Due to the abandonment of the dynamical framework, the WRF-SOM may not be able to obtain ideal prediction results in some areas dominated by local dynamic processes (e.g., surface currents, vortex, Ekman pumping, and turbulence).

305 Considering the SST characteristics in the extended-range predictions and the limitation of available computing resources, our method provides a new idea for exploring the predictability in the extended period. At present, our prediction experiments cover summer, autumn, and the first half of winter, which leads to the lack of representation of other seasons. Moreover, we do not pay too much attention to the underlying surface temperature before typhoon generation in this study, but it is an important driving factor for typhoon generation predictions. In the future, it is useful to expand the number of

310 prediction examples to cover a longer period such as one year, extend the forecast time of each case, and improve the model horizontal resolution, and further get insights on the WRF-SOM in the predictability of typhoon genesis. Finally, due to the joint impact of the initial conditions and the external forcing on the extended-range predictability of the atmosphere, we need to add the control experiments to quantitatively evaluate the effect of nonlinear errors growth in the atmosphere and external forcing differences from the ocean on the extended-range predictions.

315 **Code and data availability**

Codes, data, and scripts used to run the models and produce the figures in this work are available on the Zenodo site (https://doi.org/10.5281/zenodo.6481868, Wang et al., 2022) or by sending a written request to the

corresponding author (Shaoqing Zhang, szhang@ouc.edu.cn).

Author contributions

320 Zhenming Wang is responsible for all plots, initial analysis, and some writing; Shaoqing Zhang proposes the idea; Shaoqing Zhang leads the project, organizes and refines the paper; Yishuai Jin, and Yinglai Jia provide significant discussions and inputs for the whole research; all other co-authors make contributions by wording discussions, comments, and reading proof.

Competing interests

The authors declare that they have no conflict of interest.

Acknowledgments

The research is supported by the National Natural Science Foundation of China (Grant No. 41830964), the National Key R&D Program of China (grant No. 2022YFE0106400) and Science and Technology Innovation Project of Laoshan Laboratory (Nos. LSKJ202202200, LSKJ202202202). All numerical experiments are performed on the platforms at Laoshan Laboratory.

Reference

Wheeler, M. C., and Hendon, H. H.: An All-Season Real-Time Multivariate MJO Index: Development of an Index for Monitoring and Prediction, Monthly Weather Review, 132, 1917-1932, https://doi.org/10.1175/15200493(2004)132<1917:AARMMI>2.0.CO;2, 2004.

Vitart, F., and Robertson, A. W.: The sub-seasonal to seasonal prediction project (S2S) and the prediction of extreme events, Npj Climate and Atmospheric Science, 1, 1-7, https://www.nature.com/articles/s41612-018-0013-0, 2018.

Vitart, F.: Sub-Seasonal to Seasonal Prediction: linking weather and climate, Proc. of the World Weather Open Science Conference (WWOSC), 2014.

White, C. J., Henrik, C., Robertson, A. W., Andrew, W. R., Richard, K. Jeffrey, K. L., Arun, K., Frederic, V., Erin, C. P., Andrea J. R., Virginia M., Sukaina B., Dave M., Rachel J., Lora F., Andrew P. M., Bernd E., Richard G., Erik, K., Emily, B., Kathleen, V. P., Neil, J. H., Darryn, M., Michael, D., Sarah, P. K., Timothy, J. B., Roger, S., Lindsey, J., Tomas, A. R., IndiHodgson-Johnston, Carlo, B., Rob, L., Holger, M., Berit, A., and Stephen, E. Z.: Potential applications of sub-seasonal-to-seasonal (S2S) predictions, Meteorological Applications, 24, 1-43, https://doi.org/10.1002/met.1654, 2017.

David, A.: Current capabilities in Sub-seasonal to Seasonal Prediction, Sub-seasonal to Seasonal Prediction work shop, 2010.

345   Dian, A. P., Arthr, J. M., and Hyodae, S.: Isolating mesoscale coupled ocean-atmosphere interactions in the Kuroshio Extension region. Dynamics of Atmospheres and Oceans, 63, 60-78, https://10.0.3.248/j.dynatmoce.2013.04.001, 2013.

Stan, C.: The role of SST variability in the simulation of the MJO, Climate dynamics: Observational. theoretical and computational research on the climate system, https://link.springer.com/article/10.1007/s00382-017-4058-2, 51, 2943-2964, 2018.

350   Vitart, F.,and Molteni, F.: Dynamical Extended-Range Prediction of Early Monsoon Rainfall over India, Monthly Weather Review, 137, 1480-1492, https://journals.ametsoc.org/view/journals/mwre/137/4/2008mwr2761.1.xml, 2010.

Rashid, H. A., Hendon, H. H., Wheeler, M. C., and Alves, O.: Prediction of the Madden-Julian oscillation with the POAMA dynamical prediction system, Climate Dynamics, 36, 649-661, https://doi.org/10.1007/s00382-010.0754-x, 2011.

Saravanan, R., and Chang, P.: Midlatitude Mesoscale Ocean-Atmosphere Interaction and Its Relevance to S2S Prediction-
355   ScienceDirect, Sub-Seasonal to Seasonal Prediction, edited by: Robertson A. W., and Vitart F., Elsevier, Oxford,United Kingdom,183-200, https://doi.org/10.1016/B978-0-12-811714-9.00009-7, 2019.

Wu, D., Chen, X., and Lv, J.: The effects of finite amplitude bottom topography in a continuously stratified tropical ocean. Journal of Ocean University of Qingdao, 27,17-22, https://doi.org/10.16441/j.cnki.hdxb.1997.01.003, 1997.

Ren, X., and Qian, Y.: A coupled regional air-sea model, its performance and climate drift in simulation of the East Asian
360   summer monsoon in 1998, International Journal of Climatology, 25, 679-692, https://doi.org/10.1002/joc.1137, 2010.

Hu, Y., Song, Z., and Song, Y.: Analysis of Biases of the Simulated Tropical Indian Ocean SST in CESM1. Advances in Marine Science, 35, 350-361, https://doi.org/10.3969/j.issn.1671-6647.2017.03.005, 2017.

Li, M., Zhang, S., Wu, L., Lin, X., Chang, P., Danabasoglu, G., Wei, Z., Yu, X., Hu, H., Ma, X., Ma, W., Jia, D., Liu, X., Zhao, H., Mao, K., Ma, Y., Jiang, Y., Wang, X., Liu, G., and Chen, Y.: A high-resolution Asia-Pacific regional coupled
365   prediction system with dynamically downscaling coupled data assimilation, Science Bulletin, 65, 1849-1858, https://doi.org/10.1016/j.scib.2020.07.022, 2020.

Palmer, T. N., Brankovic, C., Molteni, F., and Tibaldi, S.: The European Centre for Medium-Range Weather Forecasts (ECMWF) Program on Extended-Range Prediction, Bulletin of the American Meteorological Society, 71, 1317-1330, https://10.1175/1520-0477(1990)071<1317:TECFMR>2.0.CO;2, 1990.

370   Zuidema, P., Chang, P., Medeiros, B., Kirtman, B., Mechoso, R., and Xu, Z.: Challenges and prospects for reducing coupled climate model SST biases in the eastern tropical Atlantic and Pacific Oceans: The U.S. CLIVAR Eastern Tropical oceans Synthesis Working Group, Bulletin of the American Meteorological Society, 197, 2305-2327, http://dx.doi.org/10.1175/BAMS-D-15-00274.1, 2016.

Saha, S., Moorthi, S., Wu, X., and Wang, J.: The NCEP Climate Forecast System Version 2, Journal of Climate, 27, 2185-
375   2208, https://doi.org/10.1175/JCLI-D-12-00823.1, 2014.

Raymond, T. P., Peter, B. R., and Rory O. R. Y. T.: The deepening of the wind-Mixed layer, Geophysical Fluid Dynamics, 4, 381-404, https://doi.org/10.1080/03091927208236105, 1973.

Jia, Y., Chang, P., and Istvan, S.: A Modeling Strategy for the Investigation of the Effect of Mesoscale SST Variability on

Atmospheric Dynamics, Geoghysical Research Letters. 46, 3982-3989, https://doi.org/10.1029/2019GL081960, 2019.

380 Wilson A. B., Bromwich H. D., and Keith M. H., Evaluation of Polar WRF forecasts on the Arctic System Reanalysis Domain:2. Atmospheric hydrologic cycle. Journal of Geophysical Research: Atmospheres, 117 (D4), 1-18, doi: 10.1029/2011JD016765, 2012.

Chen, F., and Dudhia J., Coupling an advanced land surfacehydrology model with the Penn State-NCAR MM5 modeling system. Part I. Model and implementation and sensitivity, Monthly Weather Review, 129, 569–585, doi:10.1175/1520-

385 0493(2001)1292.0.CO;2, 2001.

Skamarock, W. C., Klemp, J. B., Dudhia, J., Gill, D. O., Barker, D. M., Duda, M.G., Huang, X., Wang, W., and Powers, J. G.: A Description of the Advanced Research WRF Version 3. Ncar Technical, http://dx.doi.org/10.5065/D68S4MVH, 2008.

Shchepetkin, A. F., and Mcwilliams J. C.: The regional oceanic modeling system (ROMS): a split-explicit, free-surface,

390 topography-following-coordinate oceanic model, Ocean Modelling, 9, 347-404, https://doi.org/10.1016/j.ocemod.2004.08.002, 2005.

Li, J., and Ding, R.: Relationship between the predictability limit and initial error in chaotic systems, Chaotic Systems, edited by: Esteban T., InTechOpen, London, United Kingdom, 39-50, https:///doi.org/10.5772/13902, 2011.

Cummings, J. A., and Smedstad, O. M.: Variational Data Assimilation for the Global Ocean, Oceanic and Hydrologic

395 Applications, pp. 303-343, https://link.springer.com/chapter/10.1007/978-3-642-35088-7_13, 2013.

Srinivasan A., Chassignet E.P., Bertino L., Brankart J. M., Brasseur P., Chin T. M., Counillon F., Cummings J. A., Mariano A. J., Smedstad O. M., and Thacker W. C.: A comparison of sequential assimilation schemes for ocean prediction with the HYbrid Coordinate Ocean Model (HYCOM): Twin experiments with static forecast error covariances, 37, 85-111, https://doi.org/10.1016/j.ocemod.2011.01.006, 2011.

400 Chassignet E. P., Smith L.T., HallIwell G. R., and Bleck R., : North Atlantic Simulations with the Hybrid Coordinate Ocean Model (HYCOM): Impact of the Vertical Coordinate Choice, Reference Pressure, and Thermobaricity, Journal of Physical Oceanography, 33, 2504-2526, https://doi.org/10.1175/1520-0485(2003)033<2504:NASWTH>2.0.CO;2, 2003.

Lekshmi, S., Chattopadhyay R., Kaur M., Joseph S., Phani R., Dey A., and Sahai A.: On the role of Initial Error Growth in the Skill of Extended Range Prediction of Madden-Julian Oscillation (MJO), Theoretical and Applied Climatology, 147,

405 205-215, https://link.springer.com/article/10.1007/s00704-021-03818-3, 2022.

Yang D., Yin B., Liu Z., Bai T., Qi J., and Chen H.: Numerical study on the pattern and origins of Kuroshio branches in the bottom water of southern East China Sea in summer, Journal of Geophysical Research, 117, 1-16, 10.1029/2011jc007528, 2012.

Shell K. M.: Consistent Differences in Climate Feedbacks between Atmosphere–Ocean GCMs and Atmospheric GCMs with

410 Slab-Ocean Models, Journal of Climate, 26, 4264-4281, https://doi.org/10.1175/JCLI-D-12-00519.1, 2013.

Wu, J., Ren, H., Zuo, J., Zhao, C., Chen, L., and Li, Q.: MJO prediction skill, predictability, and teleconnection impacts in the Beijing Climate Center Atmospheric General Circulation Model, Dynamics of Atmospheres and Oceans, 75, 78-90,

https://dx.doi.org/10.1016/j.dynatmoce.2016.06.001, 2016.

Benjamin, S. G. and Daniel, R. C.: Surface heat flux parameterizations and tropical Pacific Sea surface temperature simulations. Journal of Geophysical Research, 98, 6979-6989, https://doi.org/10.1029/93JC00323, 1993.

Chen F., Shapiro G., and Thain R.: Sensitivity of Sea Surface Temperature Simulation by an Ocean Model to the Resolution of the Meteorological Forcing, 2013, 1-12, https://doi.org/10.5402/2013/215715, 2013.

Xu M., Wang Y., Zhang J., Yang D., Yin X., Gao Y., Wang G., Lv X., Data assimilation in a regional high-resolution ocean model by using Ensemble Adjustment Kalman Filter and its application during 2020 cold spell event over Asia-Pacific region, Applied Ocean Research, 129, 1-17,10.1016/J.APOR.2022.103375, 2022

Hao, S., Mao, J., and Wu, G.: Impact of air-sea interaction on the genesis of the tropical incipient vortex over south China sea: a case study, Journal of Tropical Meteorology, 22, 287-295, https://doi.org/10.16555/j.1006-8775.2016.03.003, 2016.

Zeng, G., Qi, Y., and Chen, X.: Analysis of the relationship between the intra-seasonal variabilities of SST and 850 hPa air temperature in the East China Sea and the Yellow Sea using the singular value decomposition (SVD) method, Journal of Marine Sciences, 28, 22-27, https://doi.org/1001-909X(2010)02-0022-06, 2010.

Lu, R., and Lin, Z.: Role of subtropical precipitation anomalies in maintaining the summertime meridional teleconnection over the western North Pacific and East Asia, Journal of Climate, 22, 2058-2072, https://doi.org/10.1175/2008JCLI2444.1, 2009.

Zhou, T., Yu, R., Zhang, J., Grange H., Cassou C., Deser C., Hodson D. L. R., Gomez E. S., Keenlyside N., Xin X., Okumura Y., and Li J.: Why the western Pacific subtropical high has extended westward since the late 1970s, Journal of Climate, 22, 2199-2215, https://doi.org/10.1175/2008JCLI2527.1, 2009.

Potter H., Drennan W. M., Graber H. C.: Upper ocean cooling and air-sea fluxes under typhoons: A case study[J]. Journal of Geophysical Research: Oceans, 122, 7237-7252,10.1002/2017JC012954, 2017.

Webster, P. J., Belanger, J. I., and Curry, J. A.: Extended Prediction of North Indian Ocean Tropical Cyclones Using the ECMWF Variable Ensemble Prediction System, Monitoring and Prediction of Tropical Cyclones in the Indian Ocean and Climate Change, edited by: Mohanty U. C., Mohapatra M., Singh O. P., Bandyopadhyay B. K., and Rathore L. S., Springer Dordrecht, Netherlands, 115-122, https://doi.org/10.1007/978-94-007-7720-0_11, 2014.

Anthes, R. A.: Tropical Cyclones: Their Evolution, Structure, and Effects, Meteorological Monographs, edited by Dutton J., American Meteorological Society, Boston, United States, 184-211, https://doi.org/10.1007/978-1-935704-28-7, 1982.

Holland, G. J.: Tropical cyclone motion: environment interaction plus a beta effect, Journal of Atmospheric Science, 40, 328-342, https://doi.org/10.1175/1520-0469(1983)040<0328:TCMEIP>2.0.CO;2, 1983.

450

455

460
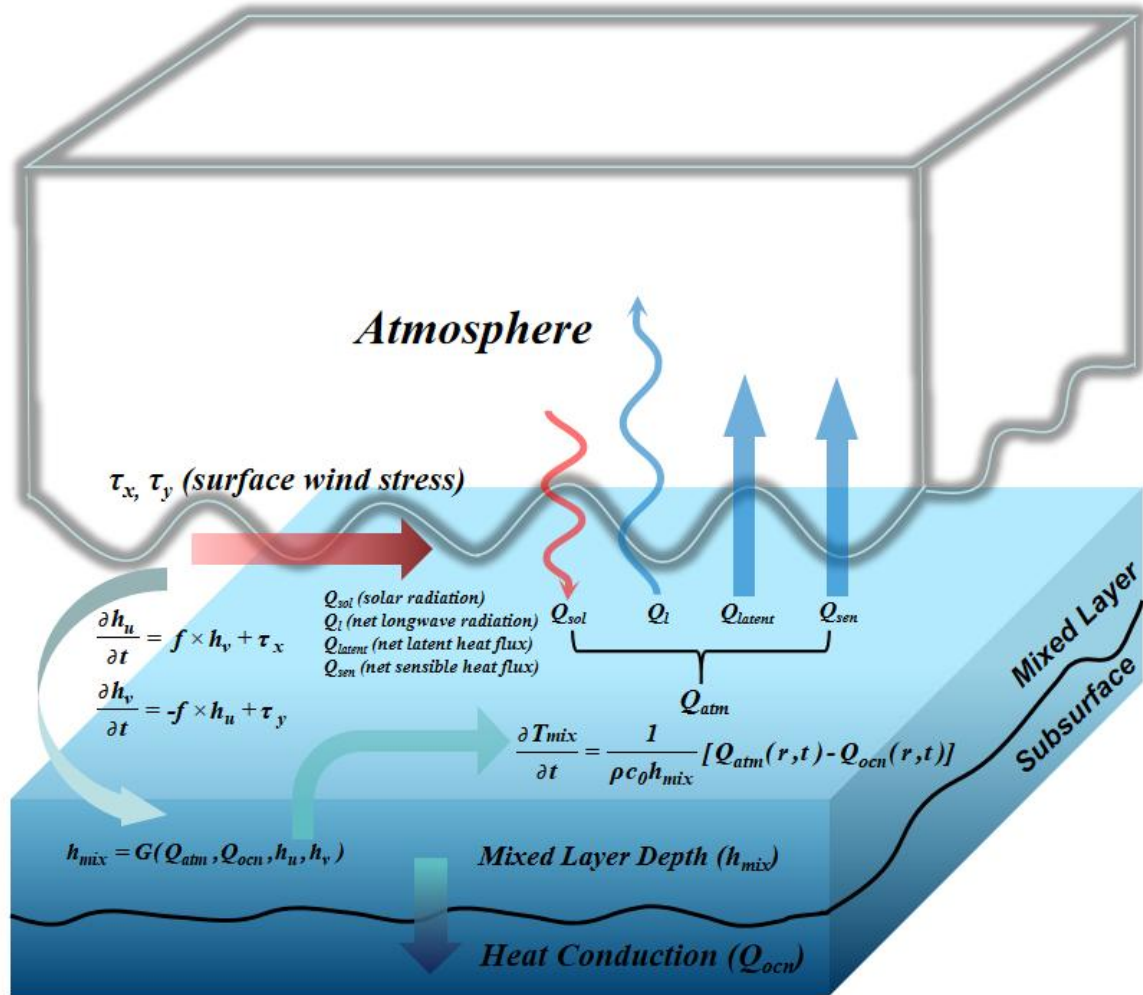
465 **Figure 1: Schematic illustration of a Slab Ocean Model (SOM) coupled to the Weather Research and Forecasting model (WRF). τ_x τ_y are respectively the zonal and meridional component of wind stress at the surface, h_u (h_v) is the τ_x-driven (τ_y-driven) momentum in the ocean mixed layer, f is Coriolis force, C_0 is the specific heat capacity of the ocean water, and h_{mix} is the mixed layer depth.**
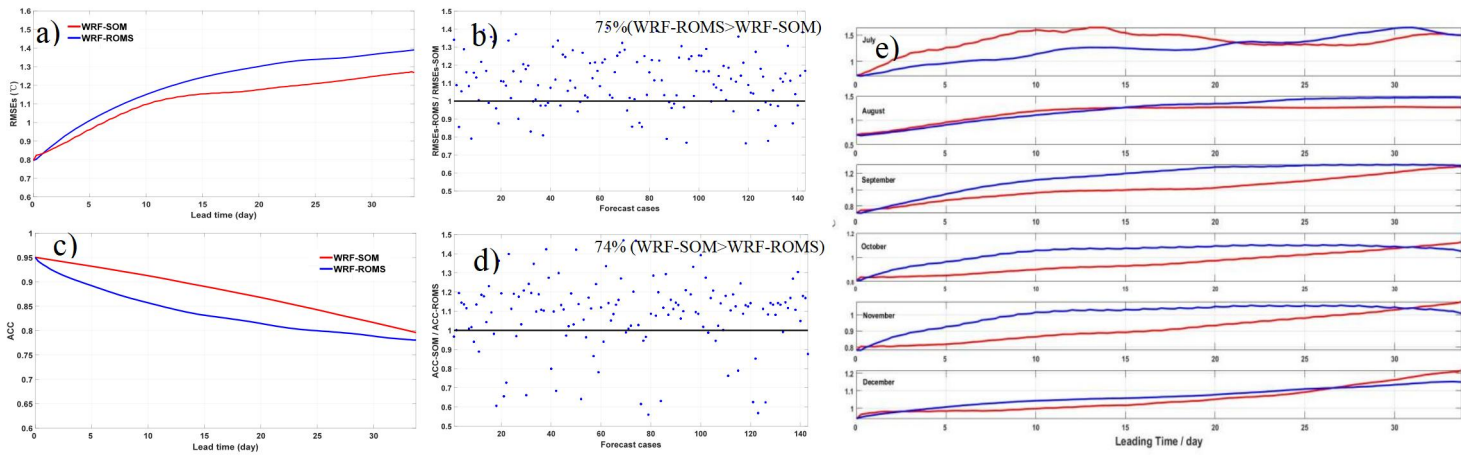
470

Figure 2: Time series of *a*) averaged root mean square errors (RMSEs), *c*) anomaly correlation coefficients (ACCs), and e) averaged RMSEs over different seasons of simulated sea surface temperatures (SSTs) against Hybrid Coordinate Ocean Model (HYCOM) reanalysis of total 142 forecast cases from July 19th to December 31st, 2020. The comparison of the *b*) RMSEs, and *d*) ACC between WRF-SOM and WRF-ROMS for each case.
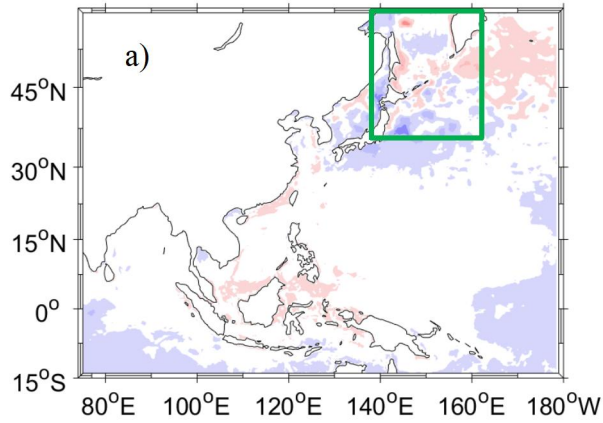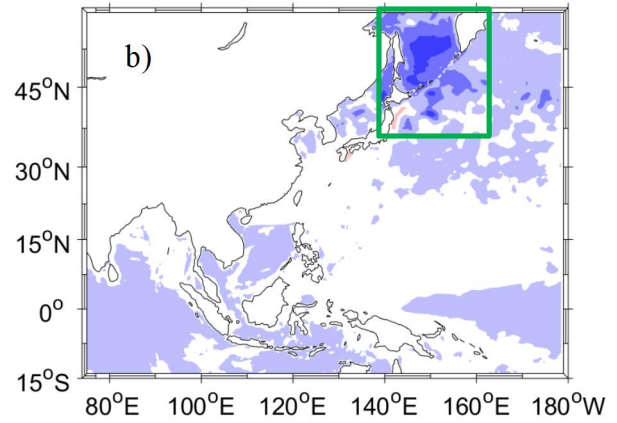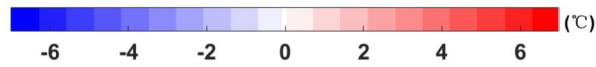
Figure 3: The spatial distributions of the SST errors of *a*) WRF-SOM, and *b*) WRF-ROMS against the HYCOM reanalysis of total 142 forecast cases from July 19th to December 31st, 2020 averaged in the 34-day forecast period. The region in green rectangle (35° N-58° N, 140° E-160° E) is the cold deviation area in WRF-ROMS.
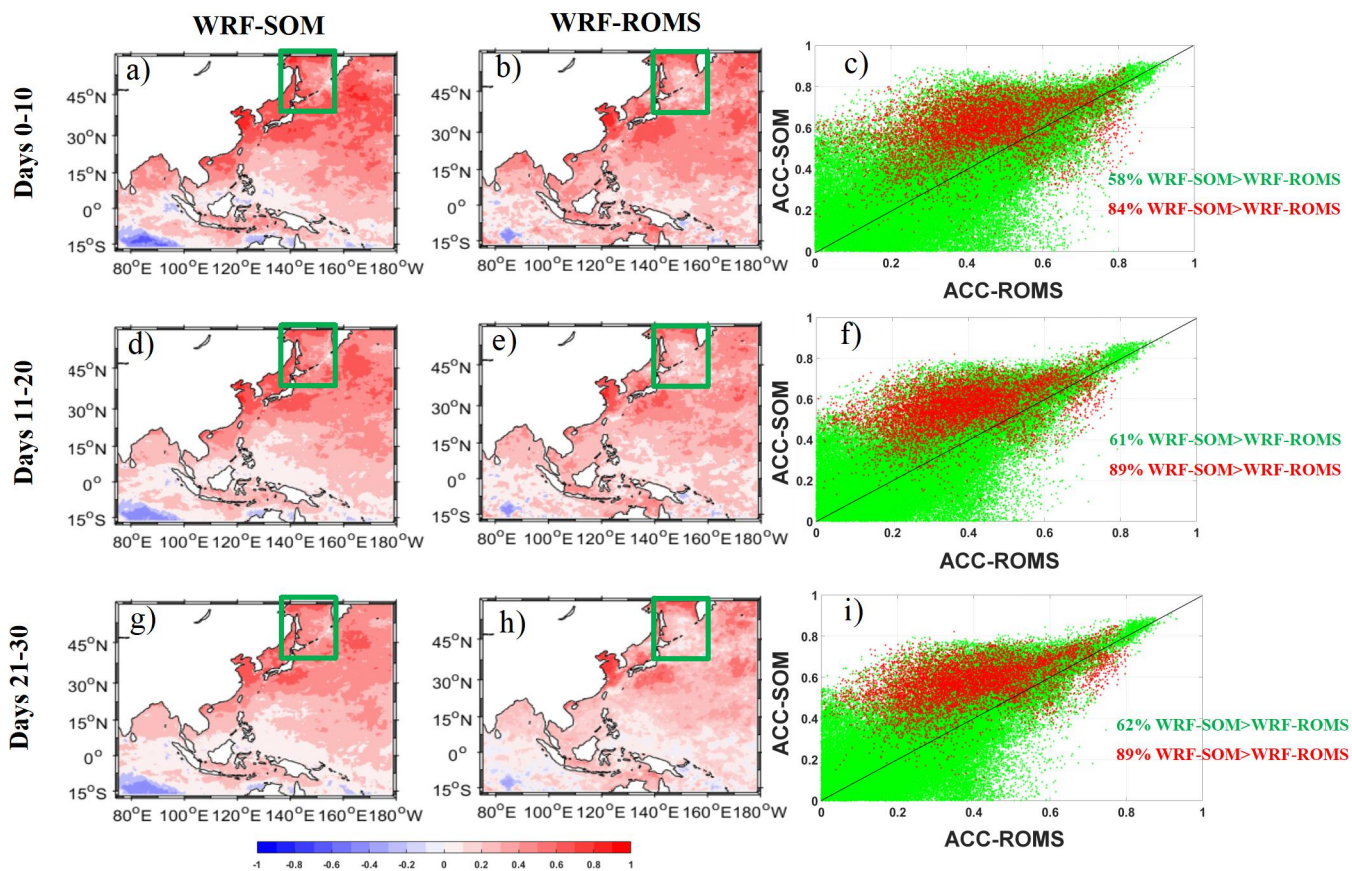
Figure 4: The spatial distributions of ACC of forecasted SSTs in the WRF-SOM (left column, panels *adg*), WRF-ROMS coupled models (middle column, panels *beh*) and their comparisons of each grid (right column, panels *cfi*) in the model domain (green dots) including cold deviation area (red dots) against HYCOM reanalysis, averaged in the first 10 days (upper panels *abc*), days 11-20 (middle panels *def*), days 21-30 (bottom panels *ghi*) forecasts of total 142 forecast cases from July 19th to December 31st, 2020.
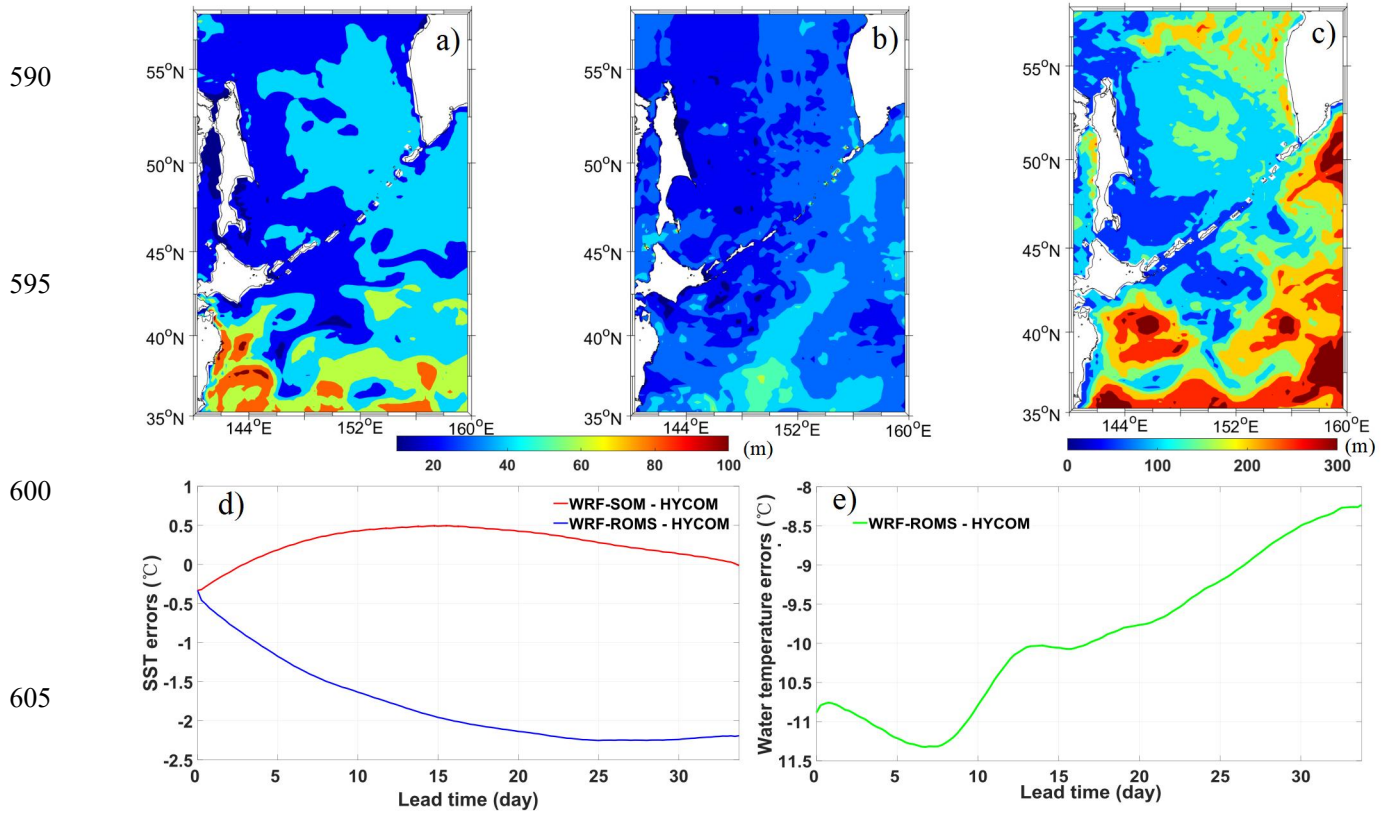
Figure 5: The spatial distribution of the mixed layer depth in the cold deviation area in the *a*) Ocean Reanalysis, *b*) WRF-SOM, and *c*) WRF-ROMS of total 142 forecast cases from July 19th to December 31st, 2020 averaged in the 34-day forecast period. The time-series of averaged water temperature errors at the *d*) surface in WRF-SOM (red) and WRF-ROMS (blue), and the *e*) subsurface (300m-400m) in WRF-ROMS (green) against HYCOM reanalysis in the cold deviation area.
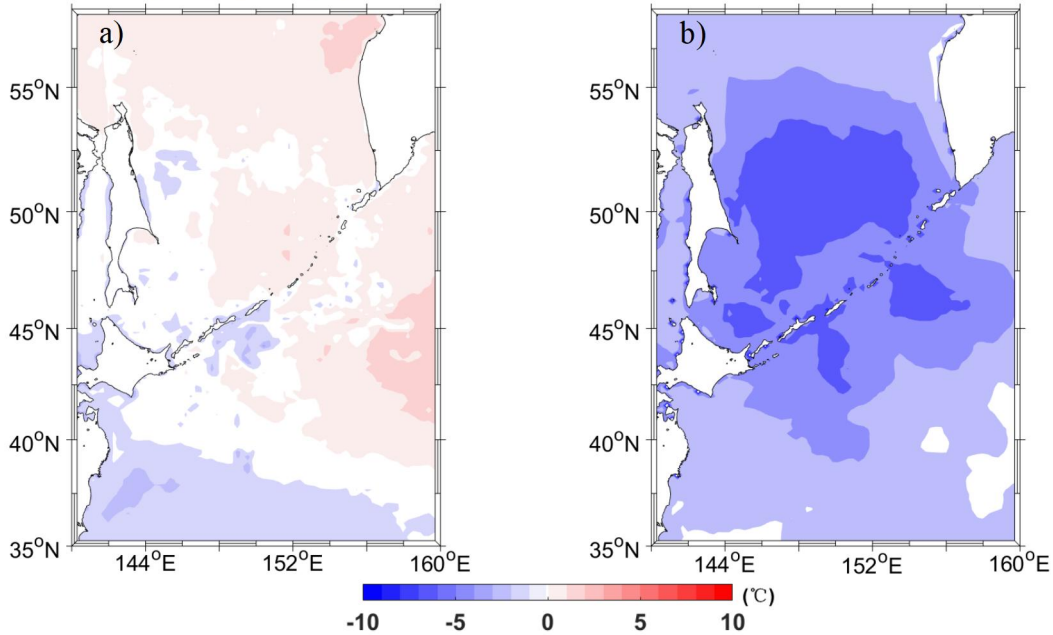
Figure 6: The spatial distribution of air temperature errors in the cold deviation area at the surface in the *a*) WRF-SOM, and *b*) WRF-ROMS against Climate Forecast System versions 2 (CFSv2) reanalysis of total 142 forecast cases from July 19th to December 31st, 2020 averaged in the 34-day forecast period.
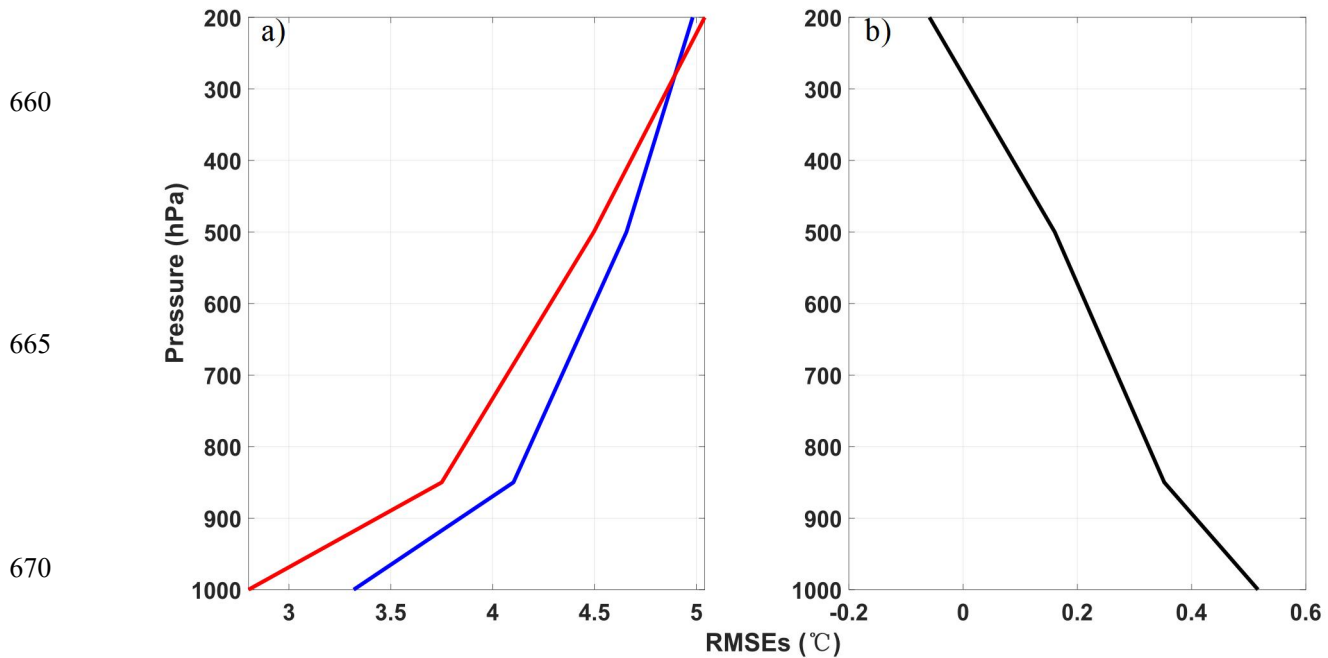
Figure 7: The *a*) variations of RMSE of air temperature with air pressure between the WRF-SOM and WRF-ROMS against the CFSv2 reanalysis averaged in the 34-day of total 142 forecast cases from July 19th to December 31st, 2020, and the *b*) variation of the difference of RMSEs in two models with the air pressure.
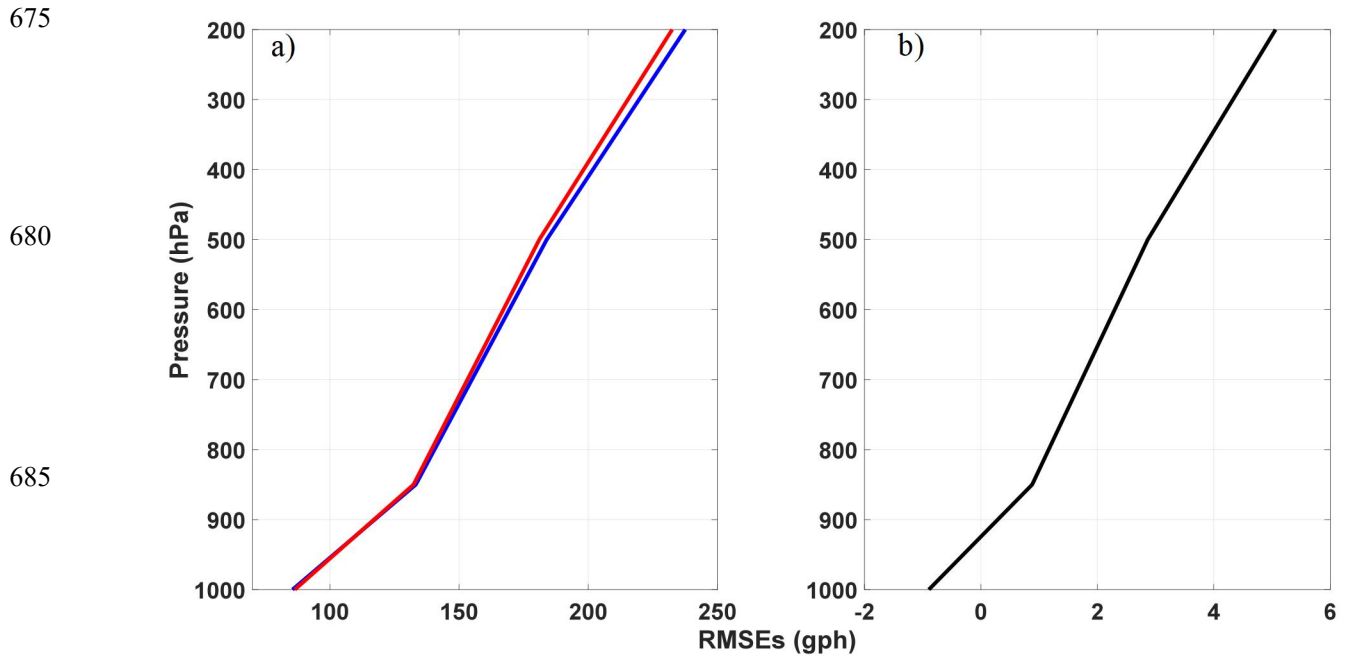
Figure 8: The *a*) variations of RMSEs of the geopotential height (GPH) with air pressure in the WRF-SOM (red) and WRF-ROMS (blue) against CFSv2 reanalysis of total 142 forecast cases from July 19th to December 31st, 2020, and the *b*) variation of the difference of RMSEs in two models with the air pressure.
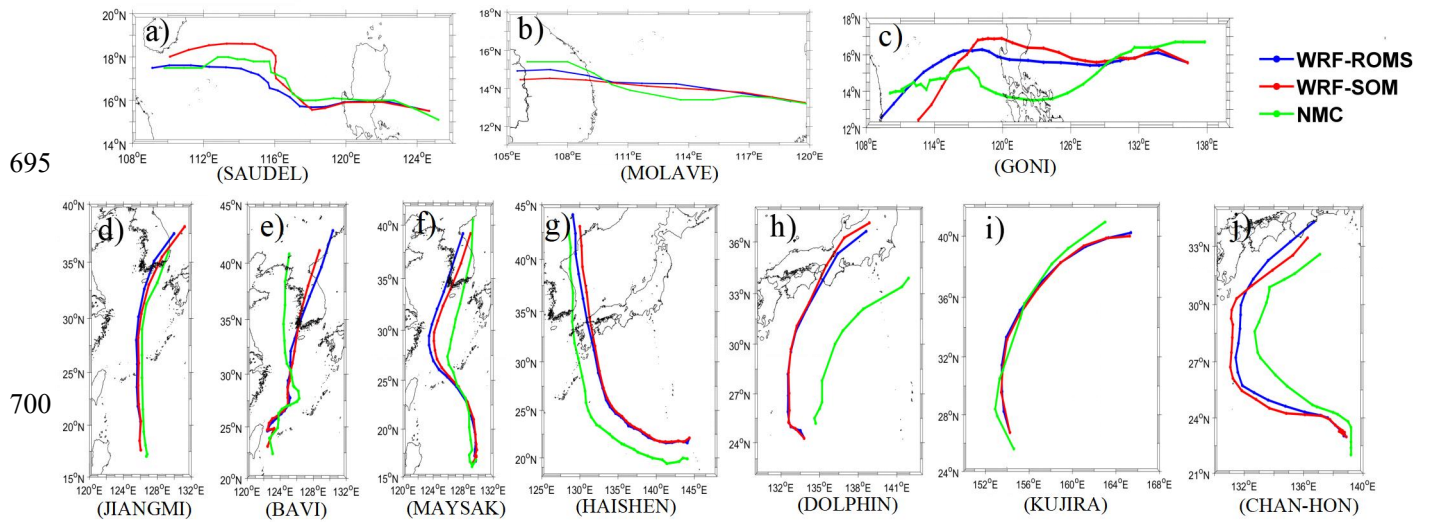
Figure 9: The typhoon tracks simulated in the WRF-SOM (red) and WRF-ROMS (blue) compared with National Meteorological Center (NMC) (green) during typhoon season (NMC data, http://typhoon.nmc.cn/web.html).
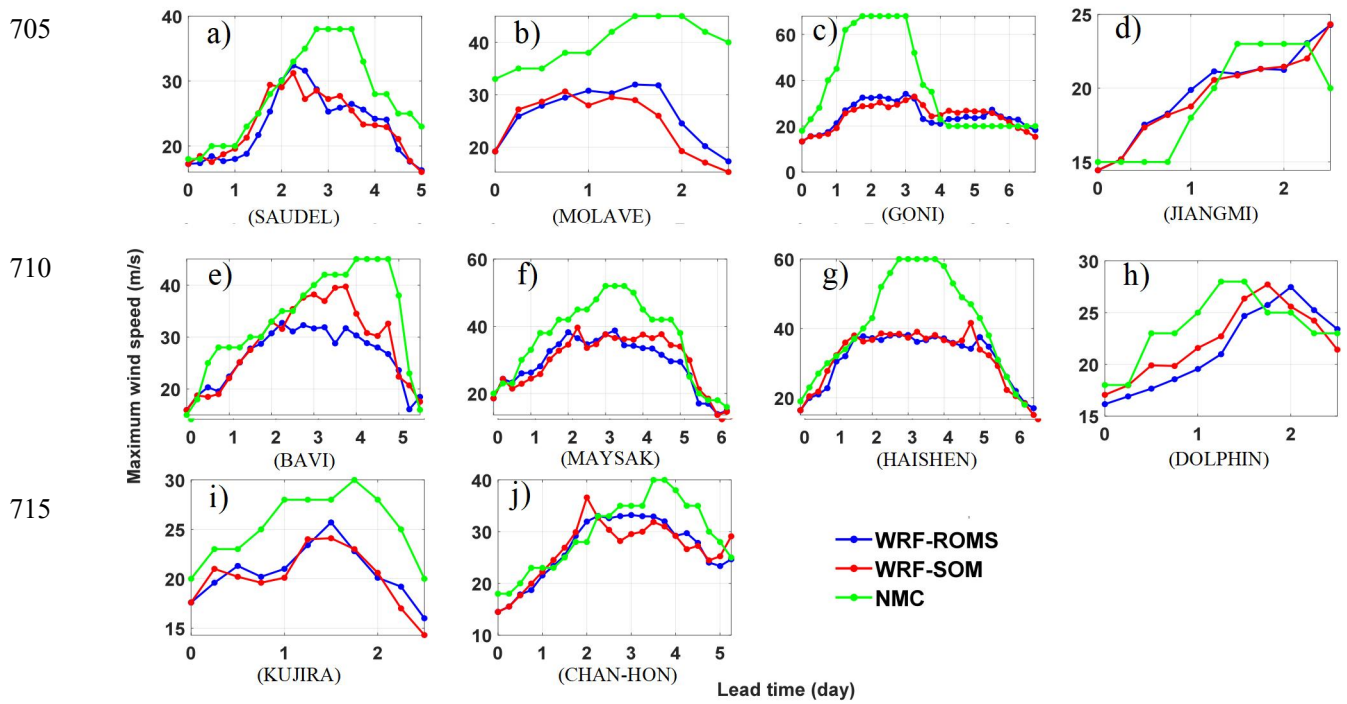
Figure 10: The maximum wind speed (MWS) of typhoon simulated in the WRF-SOM (red) and WRF-ROMS (blue) compared with National Meteorological Center (NMC) (green) during typhoon season (NMC data, http://typhoon.nmc.cn/web.html).

725 **Table 1: Typhoon track errors in different simulation periods compared with observations from NMC**

Lead time (hour)	Model	The distance of typhoon center against observations (km)
24	WRF-SOM	171
	WRF-ROMS	187
48	WRF-SOM	188
	WRF-ROMS	204
72	WRF-SOM	224
	WRF-ROMS	247